Title:

Application of copper (I) selective ligands for PET imaging of reactive oxygen species through metabolic trapping

Keywords:

Reactive oxygen species; Ferroptosis; Copper-64; Positron emission tomography

Authors:

Tetsuro Tada [a], Yuki Mizuno [b, c,*], Yuki Shibata [b], Hironobu Yasui [d,e], Yuji Kuge [b, c]

a. Graduate School of Biomedical Science and Engineering, Hokkaido University, Hokkaido 060-0815, Japan

b. Central Institute of Isotope Science, Hokkaido University, Hokkaido 060-0815, Japan

c. Global Center for Biomedical Science and Engineering, Hokkaido University, Hokkaido 060-0815, Japan

d. Faculty of Veterinary Medicine, Hokkaido University, Hokkaido 060-0818, JAPAN

e. One Health Research Center, Hokkaido University, Hokkaido 060-0818, JAPAN

*Corresponding author at: Central Institute of Isotope Science, Hokkaido University, Kita 15, Nishi 7, Kita-ku, Sapporo, Hokkaido 060-0815, Japan.

Email address: mizuno@ric.hokudai.ac.jp (Y. Mizuno)

Abstract

Introduction: Reactive oxygen species (ROS) are attractive targets for clinical PET imaging. In this study, we hypothesized that PET imaging of ROS would be possible by using chelating ligands (L) that form stable complexes with copper (I) but not with copper (II), based on metabolic trapping. Namely, when $[^{64}Cu][Cu^{I}(L)_2]^{+}$ is oxidized by ROS, the oxidized complex will release $[^{64}Cu]Cu^{2+}$. Then, the released $[^{64}Cu]Cu^{2+}$ will be trapped inside the cell, resulting in PET signal depending on the redox potential of ROS. To examine the potential of this novel molecular design for ROS imaging, we synthesized copper (I) complexes with bicinchoninic acid (BCA) disodium salt and bathocuproinedisulfonic acid (BCS) disodium salt and evaluated their reactivity with several kinds of ROS. In addition, the cellular uptake of $[^{64}Cu][Cu^{I}(BCS)_2]^{3-}$ and the stability of $[^{64}Cu][Cu^{I}(BCS)_2]^{3-}$ in a biological condition were also evaluated.

Methods: $[^{64}Cu]Cu^{2+}$ was reduced to $[^{64}Cu]Cu^{+}$ by ascorbic acid and coordinated with BCA

and BCS in the acetate buffer to synthesize $[^{64}Cu][Cu^{I}(BCA)_2]^{3-}$ and $[^{64}Cu][Cu^{I}(BCS)_2]^{3-}$. The radiochemical yields were determined by thin-layer chromatography (TLC). After $[^{64}Cu][Cu^{I}(BCS)_2]^{3-}$ was incubated with hydroxyl radical, lipid peroxide, superoxide, and hydrogen peroxide, the percentage of released $[^{64}Cu]Cu^{2+}$ from the parent complex was evaluated by TLC. HT-1080 human fibrosarcoma cells were treated with 0.1% Dimethyl sulfoxide (control), imidazole ketone erastin (IKE), or IKE + ferrostatin-1 (Fer-1). Then, the uptake of $[^{64}Cu][Cu^{I}(BCS)_2]^{3-}$ to HT-1080 cells in each group was evaluated as %Dose/mg protein. Lastly, $[^{64}Cu][Cu^{I}(BCS)_2]^{3-}$ was incubated in human plasma, and its intact ratio was determined by TLC.

Results: The radiochemical yield of $[^{64}Cu][Cu^{I}(BCS)_2]^{3-}$ (86 ± 1%) was higher than that of $[^{64}Cu][Cu^{I}(BCA)_2]^{3-}$ (44 ± 3%). $[^{64}Cu][Cu^{I}(BCA)_2]^{3-}$ was unstable and partially decomposed on TLC. After $[^{64}Cu][Cu^{I}(BCS)_2]^{3-}$ was reacted with hydroxyl radical, lipid peroxide, and superoxide, 67 ± 2%, 44 ± 13%, and 22 ± 3% of total radioactivity was detected as $[^{64}Cu]Cu^{2+}$, respectively. On the other hand, the reaction with hydrogen peroxide did not significantly increase the ratio of $[^{64}Cu]Cu^{2+}$ (4 ± 1%). These results suggest that $[^{64}Cu][Cu^{I}(BCS)_2]^{3-}$ could be used for detecting high-redox-potential ROS such as hydroxyl radical and lipid peroxide with high selectivity. The cellular uptake values of $[^{64}Cu][Cu^{I}(BCS)_2]^{3-}$ in the control, IKE, and Fer-1 group were 42 ± 2, 54 ± 2, and 47 ± 5%Dose/mg protein (n = 3), respectively, suggesting the ROS specific uptake of $[^{64}Cu][Cu^{I}(BCS)_2]^{3-}$. On the other hand, the intact ratio after the incubation of $[^{64}Cu][Cu^{I}(BCS)_2]^{3-}$ in human plasma was 9 ± 5%.

Conclusion: PET imaging of ROS would be possible by using a copper (I) selective ligand, based on metabolic trapping. Although improvement of the membrane permeability and the stability of copper (I) complexes is required, the present results pave the way for the development of novel ^{64}Cu-labeled complexes for PET imaging of ROS.

1 Introduction

Reactive oxygen species (ROS) are involved in the pathogenesis and therapeutic responsiveness of various diseases, including cancer [1]. For example, many tumor cells produce a large amount of ROS through their active metabolism, and the production of ROS has been linked to the malignant transformation of tumor cells [2]. At the same time, excess production of ROS can be lethal for tumor cells, and some tumor cells enhance antioxidant pathways to avoid the toxicity imposed by an excess amount of ROS. Such an enhancement of antioxidant pathways can impair the efficacy of chemotherapy and radiotherapy [2], [3], whose anti-tumor mechanism depends on the induction of excess ROS [4], [5]. Therefore, to monitor the therapeutic efficacy of anti-tumor treatments that depend on the production of ROS, non-invasive quantification of ROS in tumor tissues is highly important, and the development of novel ROS imaging agents is urgently needed.

PET imaging is one of the most attractive imaging modalities due to its high resolution and sensitivity. The most common strategy employed for PET imaging of ROS is metabolic trapping, where radiolabeled compounds are oxidized by ROS and their oxidized counterparts are trapped in ROS-rich cells. Indeed, most ROS imaging probes developed so far rely on metabolic trapping for their accumulating mechanism to ROS-rich tissues [6], [7], [8], [9], [10]. For example, ^{18}F-ROStrace is a derivative of dihydroethidium and can freely cross the cell membrane due to its neutral charge [6]. Upon oxidization by ROS, the charge of ^{18}F-ROStrace changes to positive, and the oxidized counterpart is trapped inside ROS-rich cells due to its poor membrane permeability. Therefore, ^{18}F-ROStrace highly accumulates into ROS-rich tissues, allowing the non-invasive measurement of ROS levels by PET imaging. However, while the potential of these ^{18}F-labeled ROS imaging agents has been well demonstrated in preclinical experiments, they often suffer from low radiochemical yields and complicated synthetic procedures, derived from the nature of ^{18}F radiochemistry. Indeed, the radiochemical yield of ^{18}F-ROStrace was only 8 to 12 % (decay-corrected) with a relatively long synthesis time (65 min) [6].

Radiochemistry of metallic radionuclides is quite different from that of ^{18}F and radiolabeling reactions of metallic radionuclides provide radiolabeled complexes with high radiochemical yields in short reaction time [11], [12], [13]. Therefore, it would be practically useful if metallic radionuclide complexes can be used for PET imaging of ROS. However, almost no metallic radionuclide complexes have been evaluated as a ROS imaging agent. The exception is ^{68}Ga-Galuminox, but its uptake mechanism to ROS-rich tissues is not yet determined [14].

Copper-64 (^{64}Cu) is one of the attractive metallic radionuclides for the application in clinical PET imaging due to its ideal physical property. Furthermore, copper has a rich coordination and redox chemistry, which can be exploited for the development of metabolic-trapping imaging agents. A typical example is [^{64}Cu]Cu-diacetyl-bis(N^4-methylthiosemicarbazone) ([^{64}Cu]Cu-ATSM). [^{64}Cu]Cu-ATSM is a successful PET imaging agent for over-reductive environments and accumulates into tissues with

over-reductive environment through metabolic trapping [15]. In brief, [^{64}Cu]Cu in [^{64}Cu]Cu-ATSM is reduced from Cu^{II} to Cu^{I} in over-reductive environment and disassociates from ATSM. As a result, [^{64}Cu]Cu^{I} is trapped in the cell, leading to the enhanced PET signal from tissues in over-reductive environments.

Encouraged by the success of [^{64}Cu]Cu-ATSM, we hypothesized that PET imaging of ROS based on metabolic trapping would be possible by using chelators that form stable complexes with Cu^{I} but not with Cu^{II}. Figure 1 shows a schematic illustration of the proposed ROS imaging strategy, and "L" denotes a ligand that forms a stable complex with Cu^{I} but not with Cu^{II}. According to our hypothesis, when [^{64}Cu][$Cu^{I}(L)_2$]$^{+}$ is oxidized by ROS, the oxidized complex will immediately release [^{64}Cu]Cu^{2+} due to the poor stability of the complex. Then, the released [^{64}Cu]Cu^{2+} ion will be scavenged by intracellular proteins and be trapped inside the cell, resulting in PET signal depending on the redox potential and concentration of ROS. To the best of our knowledge, there have been no reports on the application of copper (I) selective ligands for PET imaging of ROS through metabolic trapping.

In this study, to examine the potential of this novel molecular design for ROS imaging, we synthesized copper complexes with [2,2'-biquinoline]-4,4'-dicarboxylic acid (BCA) disodium salt and 2,9-dimethyl-4,7- diphenyl-1,10-phenanthrolinedisulfonic acid (BCS) (Figure 2) and evaluated their reactivity with several kinds of ROS and their stability in biological condition. As a proof-of-concept experiment, we also evaluated the uptake of [^{64}Cu][$Cu^{I}(BCS)_2$]$^{3-}$ to cancer cells with elevated ROS levels.

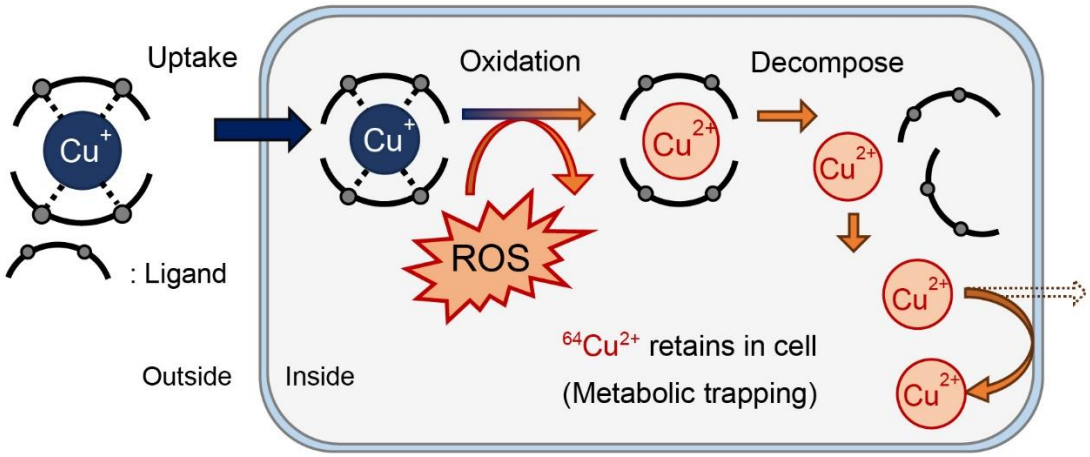

Fig. 1. The principle of ROS imaging using a chelator that is selective to Cu (I).

2 Materials and methods

2.1 General

Unless otherwise stated, all reagents were purchased from FUJIFILM Wako Pure Chemical (Osaka,

Japan). The purity of the reagents was extra-pure or higher grade unless otherwise stated. Ultrapure water was obtained Direct-Q UV3 (Merck-Millipore, Billerica, MA). Reversed-phase thin-layer chromatography (RP-TLC) analysis was performed using TLC Silica gel 60 RP-18 F_{254}s (Merck, Darmstadt, Germany). Normal phase thin-layer chromatography (TLC) analysis was performed using TLC Silica gel 60 F_{254}s (Merck, Darmstadt, Germany). High-performance liquid chromatography (HPLC) analyses were performed on Shimazu system (LC-20AD, Shimadzu Co., Kyoto, Japan) equipped with a UV/Vis and radio-detector. UV absorbance was measured at 254 nm. Radioactivity was monitored using an in-line NaI(Tl) radio-detector (Gabi star®, Elysia Raytest Co., Straubenhardt, Germany). HPLC analyses were performed with a reverse phase column (Cosmosil 5C_{18}-AR-II, 5 μm, 4.6 × 150 mm, Nacalai Tesque Inc., Kyoto, Japan) at a 1 mL/min flow rate.

Two ligands, [2,2'-biquinoline]-4,4'-dicarboxylic acid (BCA) disodium salt and 2,9-dimethyl -4,7-diphenyl-1,10-phenanthrolinedisulfonic acid (BCS) disodium salt were used in this study (Figure 2).

Statistical analyses were performed using GraphPad Prism 7 (GraphPad Software, San Diego, CA).

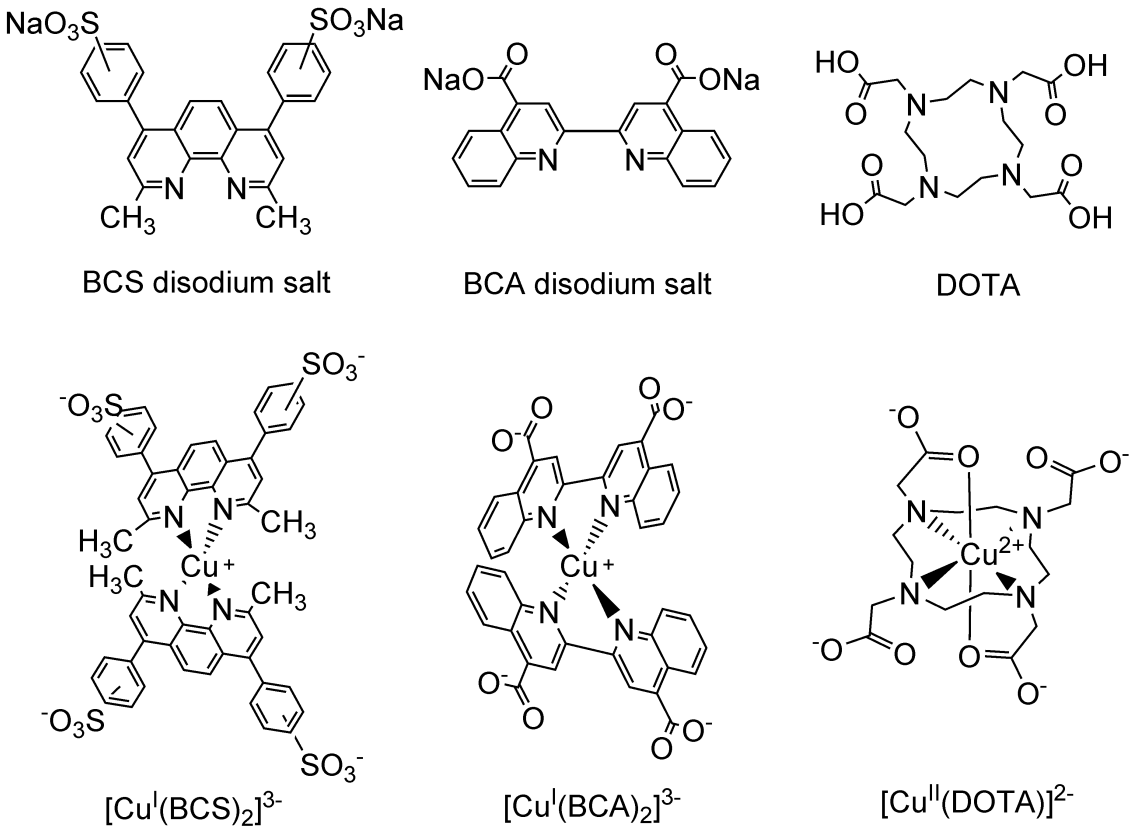

Fig. 2. Chemical structures of ligands and copper complexes used in this study.

2.2 Synthesis of natural copper complexes: [^{nat}Cu][Cu^{I}(BCA)$_2$]$^{3-}$ and [^{nat}Cu][Cu^{I}(BCS)$_2$]$^{3-}$

$[^{nat}Cu][Cu^{I}(BCA)_2]^{3-}$ was synthesized according to the method of Sato et al [16]. Briefly, 35.8 mg (92 μmol) BCA disodium salt (>98%, Tokyo Chemical Industry, Tokyo, Japan) was suspended in 1.84 mL of dimethyl sulfoxide (DMSO) and was dissolved by sonication. Separately, 3.8 mg (38 μmol) of copper(I) chloride (>95%, Junsei Chemical, Tokyo, Japan) was added to a 10 mL flask under N_2 atmosphere (>99.99%, Air Water, Tokyo, Japan). Then, 1.31 mL of the BCA solution (BCA disodium salt: 76 μmol) was added to the flask at room temperature while stirring. The color of the solution immediately changed to purple. Stirring was terminated after 15 min. On the RP-TLC analysis, the Rf value of $[^{nat}Cu][Cu^{I}(BCA)_2]^{3-}$ was 0.90 (Table 1 and Figure 5). On the HPLC analysis, the retention times of BCA and $[^{nat}Cu][Cu^{I}(BCA)_2]^{3-}$ were 6.1 and 10.3 min, respectively (Table 2, Figures S3, and S4). This reaction solution was used as the $[^{nat}Cu][Cu^{I}(BCA)_2]^{3-}$ stock solution for further experiments without purification. ESI-MS: calculated for $C_{40}H_{21}CuN_4O_8$, 374.03; found 375.05 $[M - 3H]^{2-}$ (Figure S1).

$[^{nat}Cu][Cu^{I}(BCS)_2]^{3-}$ was synthesized according to the method of Sato et al [16]. Briefly, 41.8 mg (74 μmol) of BCS disodium salt (Tokyo Chemical Industry) was dissolved in 1.48 mL of DMSO. Separately, 3.4 mg (34 μmol) of copper(I) chloride was added to a 10 mL flask under N_2 atmosphere (>99.99%, Air Water). Then, 1.36 mL of the BCS solution (BCS disodium salt: 68 μmol) was added to the flask at room temperature with stirring. The color of the solution immediately changed to brown. Stirring was terminated after 15 min. On the RP-TLC analysis, the Rf value of $[^{nat}Cu][Cu^{I}(BCS)_2]^{3-}$ was 0.80 (Table 1 and Fig. 5). On the HPLC analysis, BCS was eluted as multiple peaks, ranging from 7.8 to 10.9 min, due to the presence of substitution isomers (Table 2 and Figure S6). As a result, $[^{nat}Cu][Cu^{I}(BCS)_2]^{3-}$ was also eluted as multiple peaks, ranging from 11.9 to 15.5 minutes (Figure S7). This reaction solution was used as the $[^{nat}Cu][Cu^{I}(BCS)_2]^{3-}$ stock solution for further experiments without purification. ESI-MS: calculated for $C_{52}H_{36}CuN_4NaO_{12}S_4$, 561.02; found 561.06 $[M - 3Na]^{2-}$ (Figure S2).

Table 1 TLC analytical conditions and Rf values of copper complexes used in this study.

Complex	TLC phase	Mobile phase	Rf value
$[Cu^{I}(BCA)_2]^{3-}$	Reverse phase	Methanol/0.1 M acetate buffer (pH 5) = 6 : 4 (v : v)	0.90
$[Cu^{I}(BCS)_2]^{3-}$	Reverse phase	Methanol/0.1 M acetate buffer (pH 5) = 6 : 4 (v : v)	0.80
$[Cu^{II}(DOTA)]^{2-}$	Normal phase	1 M ammonium acetate/Methanol = 1 : 1 (v : v)	0.40

Table 2 HPLC analytical condition and retention time of copper complexes used in this study.

Complex	Solvent A	Solvent B	Gradient	Retention time [min]
$[Cu^{I}(BCA)_2]^{3-}$	10 mM Phosphate buffer (pH 6)	MeOH	10-40-40% (0-10-15 min)	10.3
$[Cu^{I}(BCS)_2]^{3-}$	10 mM Phosphate	MeOH	40-40-60%	11.9-15.5

	buffer (pH 6)		(0-5-20 min)	

2.3 Generation of ROS

Hydroxyl radical (•OH) was generated by dissolving 9 U (50 μg) of horseradish peroxidase in 1 mL of 2 or 10 mM H_2O_2 solution, prepared from 35.4 wt% (11.7 M) H_2O_2 diluted with 0.1M acetate buffer (pH 5) [17]. Lipid peroxide (LOOH) was generated according to the method of Azuma et al. [18]. Briefly, 3.1 μL (10 μmol) linoleic acid and 4 μL of 10% Tween-20 (for biochemistry, Sigma, St. Louis, MO) in 0.1 M borate buffer (pH 9), were diluted to 1 or 5 mL with 0.1 M borate buffer (pH 9). The linoleic acid was emulsified using ultrasound and vortexing. One milliliter of this linoleic acid solution was added to 8,428U (50 μg) of soybean lipoxygenase (Sigma) to generate LOOH. Superoxide ($O_2^{\bullet-}$) was generated by dissolving 0.71 mg potassium superoxide (Sigma) with 1 or 5 mL 0.1 M acetate buffer (pH 5) [19].

Hydroxyl radical (•OH) generation was confirmed using hydroxyphenyl fluorescein [20]. Briefly, 10 μM hydroxyphenyl fluorescein (HPF) solution was prepared by diluting hydroxyphenyl fluorescein (5 mM DMF solution, Goryo Chemical, Sapporo, Japan) with D-PBS. To wells in a 96-well plate, 100 μL of 10 μM HPF solution was added. Then, 100 μL of 2 mM H_2O_2 or •OH solution was added to the wells. After incubation at 37°C for 1 hour, a fluorescence signal (528 nm) from each well was measured using a plate reader (POWER SCAN HT, DS Pharma Biomedical, Tokyo, Japan). The excitation wavelength was 485 nm.

Lipid peroxide (LOOH) generation was confirmed by BODIPY 581/591 C11 [21]. Briefly, 20 μM BODIPY 581/591 C11 solution was prepared by dissolving BODIPY 581/591 C11 (Thermo Fisher Scientific, Waltham, MA) with ultrapure water. To wells in a 96-well plate, 100 μL of 20 μM BODIPY 581/591 C11 solution was added. Then, 100 μL of 2 mM LOOH solution was added to the wells. After incubation at 37°C for 1 hour, a fluorescence signal (528 nm) from each well was measured using a plate reader. The excitation wavelength was 485 nm.

Superoxide ($O_2^{\bullet-}$) was confirmed by dihydroethidium [17]. Briefly, 300 μM dihydroethidium (DHE) solution was prepared by dissolving DHE (for Biochemistry, Fujifilm Wako Pure Chemicals) with ultrapure water. To wells in a 96-well plate, 100 μL of 300 μM DHE solution was added. Then, 100 μL of 2 mM $O_2^{\bullet-}$ solution was added to the wells. After incubation at 37°C for 1 hour, a fluorescence signal (590 nm) from each well was measured using a plate reader. The excitation wavelength was 485 nm.

2.4 Reaction of $[^{nat}Cu][Cu^{I}(BCA)_2]^{3-}$ and $[^{nat}Cu][Cu^{I}(BCS)_2]^{3-}$ with ROS

$[^{nat}Cu][Cu^{I}(BCA)_2]^{3-}$ and $[^{nat}Cu][Cu^{I}(BCS)_2]^{3-}$ were reacted with hydroxyl radicals (•OH), lipid peroxide (LOOH), superoxide ($O_2^{\bullet-}$) and hydrogen peroxide (H_2O_2). First, $[^{nat}Cu][Cu^{I}(BCA)_2]^{3-}$ or

$[^{nat}Cu][Cu^{I}(BCS)_2]^{3-}$ stock solution was diluted to 100 μM with 0.1M acetate buffer (pH 5). Then, 100 μL of these solutions were added to wells of a 96-well plate (n =3). Next, 100 μL of 2 mM ROS (ROS concentration was defined by the concentration of substrates) solution was added to each well. After incubation at 37°C for 30 min, the absorbances ($[^{nat}Cu][Cu^{I}(BCA)_2]^{3-}$, 562 nm [22]; $[^{nat}Cu][Cu^{I}(BCS)_2]^{3-}$, 492 nm [23]) were measured with a plate reader (Absobance96, Byonoy GmbH, Hamburg, Germany).

2.5 Synthesis of ^{64}Cu-labeled complexes: $[^{64}Cu][Cu^{I}(BCA)_2]^{3-}$, $[^{64}Cu][Cu^{I}(BCS)_2]^{3-}$, and $[^{64}Cu][Cu^{II}(DOTA)]^{2-}$

For the synthesis of $[^{64}Cu][Cu^{I}(BCA)_2]^{3-}$ and $[^{64}Cu][Cu^{I}(BCS)_2]^{3-}$, 10 μL of 2 mM BCA disodium salt or BCS disodium salt aqueous solution was added to a 500 μL plastic tube containing 77 μL of 0.1 M acetate buffer (pH 5) and 10 μL of 1 mM sodium L-ascorbate aqueous solution. Then, 2 μL of 5% sodium dodecyl sulfate (SDS) aqueous solution was added. Finally, 1 μL (approximately 1 MBq) of $[^{64}Cu]Cu^{2+}$ solution (PDR Pharma, Tokyo, Japan) diluted with the same volume of 0.05 M HCl (for ICP, Kanto Chemical) was added, and the mixture was heated at 60°C for 10 min. After heating, 1 μL of the solution was spotted on RP-TLC and the RP-TLC was developed by a mobile phase (Table 1). Autoradiography (ARG) was obtained using phosphor imaging plates (BAS-TR 2025, Fuji Film, Tokyo, Japan) and an image analysis system (LAS7000, Multi Gauge V 3.0, Fuji Film). Radiochemical yields were determined using Multi Gauge V 3.0. The reaction solutions were analyzed by HPLC under the same conditions as for the non-radioactive copper complexes (Figures S5 and S8). For the synthesis of $[^{64}Cu][Cu^{II}(DOTA)]^{2-}$, 10 μL of 2 mM 2,2′,2′′,2′′′-(1,4,7,10-tetraazacyclododecane-1,4,7,10-tetrayl) tetraacetic acid (DOTA: Macrocycles, Plano, TX) aqueous solution was added to a 500 μL plastic tube containing 77 μL of 0.1 M acetate buffer (pH 5) and 10 μL of ultrapure water. Then, 2 μL of 5% SDS aqueous solution was added. Finally, 1 μL (approximately 1 MBq) of $[^{64}Cu]Cu^{2+}$ solution was added, and the mixture was heated at 60°C for 10 min. After heating, 1 μL of the solution was spotted on normal phase TLC and the TLC was developed by a mobile phase (Table 1). The radiochemical yield was calculated as in the case of $[^{64}Cu][Cu^{I}(BCA)_2]^{3-}$ and $[^{64}Cu][Cu^{I}(BCS)_2]^{3-}$.

2.6 Dilution stability of $[^{64}Cu][Cu^{I}(BCA)_2]^{3-}$, $[^{64}Cu][Cu^{I}(BCS)_2]^{3-}$, and $[^{64}Cu][Cu^{II}(DOTA)]^{2-}$

The solution of $[^{64}Cu][Cu^{I}(BCA)_2]^{3-}$, $[^{64}Cu][Cu^{I}(BCS)_2]^{3-}$, and $[^{64}Cu][Cu^{II}(DOTA)]^{2-}$ (approximately 1 MBq per 100 μL, ligand concentration 200 μM) was diluted 2, 10, and 100 fold with 0.1 M acetate buffer (pH 5, containing 0.1% SDS) to reach the final ligand concentration of 100, 20, and 2 μM, respectively. After dilution, the solutions were stirred by pipetting, allowed to stand for 5 minutes at

room temperature, and the percentages of the intact complex were analyzed using RP-TLC (Table 1).

2.7 Reaction of $[^{64}Cu][Cu^{I}(BCS)_2]^{3-}$ with ROS

$[^{64}Cu][Cu^{I}(BCS)_2]^{3-}$ was reacted with $^{\bullet}OH$, LOOH, $O_2^{\bullet-}$, and H_2O_2. To a 500 μL plastic tube, 10 μL of 10 mM ROS (ROS concentration was defined by the concentration of substrates) and 80 μL of 0.1 M acetate buffer (pH 5) were added. Then, 10 μL of $[^{64}Cu][Cu^{I}(BCS)_2]^{3-}$ (approximately 100 kBq, BCS disodium salt concentration 200 μM) was added, and the solution was incubated at 37°C for 30 min. After the reaction, the solution was analyzed by RP-TLC (Table 1), and percentage of the origin (*Rf*: 0.0) was calculated. The control solution was prepared by 10 fold dilution of $[^{64}Cu][Cu^{I}(BCS)_2]^{3-}$ with 0.1 M acetate buffer (pH 5). Each ROS was generated by the same method as in the case of $[^{nat}Cu][Cu^{I}(BCA)_2]^{3-}$ and $[^{nat}Cu][Cu^{I}(BCS)_2]^{3-}$. Additionally, $[^{64}Cu][Cu^{I}(BCS)_2]^{3-}$ was reacted with enzymes alone as a control experiment.

2.8 Cell Culture

HT-1080 human fibrosarcoma cells were purchased from the American Type Culture Collection (Manassas, VA). The cells were grown in the high-glucose Dulbecco's Modified Eagle medium (with L-Glutamine and Phenol Red, Wako) supplemented with 10% fetal bovine serum (CELLect®, MP Biomedicals, Santa Ana, CA) and 1% v/v penicillin-streptomycin (10,000 unit-10 mg/mL, Wako) The cells were maintained at 37°C in 5% CO_2.

2.9 Induction of cellular lipid peroxides by imidazole ketone erastin

Imidazole ketone erastin (IKE) and Ferrostatin-1 (Fer-1) were purchased from Selleckchem (Huston, TX) and Sigma-Aldrich, respectively. HT-1080 cells were seeded in type I collagen-coated 8-well slides (Corning Inc., Corning, NY) at a density of 3.6×10^4 cells per well and allowed to attach overnight. Next day, the cells were incubated in the growth medium containing 10 μM IKE alone or 10 μM IKE + 1 μM Fer-1 at 37°C for 6 h in 5% CO_2. After the incubation, the cells were washed twice with Hank's balanced salt solution (HBSS) buffer and incubated with 10 μM BODIPY C11 581/591 in HBSS buffer at 37°C for 30 minutes. After the incubation, the cells were washed twice with 500 μL HBSS buffer, and fluorescence signal of BODIPY C11 581/591 and its oxidized form, Ox-BODIPY C11, were measured. The images were obtained with a fluorescence microscope (Biozero BZ-8000, KEYENCE, Osaka, Japan) with a Plan Apo 4x objective (NA0.20, Nikon, Tokyo, Japan). The fluorescence of BODIPY C11 and Ox-BODIPY C11 were detected using TRITC filter (ex: 545/25 nm, em: 605/55 nm, dichroic: 565nm, KEYENCE) and GFP-B filter (ex: 470/40 nm, em: 535/50 nm, dichroic: 495 nm, KEYENCE), respectively.

2.10 In vitro cell uptake test of $[^{64}Cu][Cu^{I}(BCS)_2]^{3-}$

For this cellular uptake experiment, $[^{64}Cu][Cu^{I}(BCS)_2]^{3-}$ was synthesized in the same method as described elsewhere, except that the BCS concentration was 2 mM. The radiochemical yield of $[^{64}Cu][Cu^{I}(BCS)_2]^{3-}$ under this condition was over 90%. HT-1080 cells were seeded at a density of 1 × 10^5 cells per well in Type I collagen-coated plates (AGC TECHNO GLASS Co., Ltd., Shizuoka, Japan) and allowed to attach overnight. Next day, the cells were incubated in the growth medium containing 10 μM IKE alone or 10 μM IKE + 1 μM Fer-1 at 37°C for 6 h in 5% CO_2. After the incubation, the cells were washed twice with HBSS buffer and were incubated with $[^{64}Cu][Cu^{I}(BCS)_2]^{3-}$ (10 kBq. [BCS] = 8 μM) in HBSS buffer at 37°C for 30 min. The total incubation volume was adjusted to 500 μL. After the incubation, each well was washed twice with 500 μL ice-cold HBSS buffer. The cells were lysed by 15 min incubation with 0.25 M NaOH containing 0.1% SDS at 37°C, and the radioactivity was determined using an autowell γ counter (2480 WiZARD^2, PerkinElmer, Waltham, MA). The protein concentration of each cell lysate was determined using micro-BCA assay kit (Thermo Fisher Scientific) following the product instructions. The results are presented as percentage dose per milligram protein (% dose/mg protein).

2.11 Stability of $[^{64}Cu][Cu^{I}(BCS)_2]^{3-}$ in neutral solution and human plasma

To test the stability of $[^{64}Cu][Cu^{I}(BCS)_2]^{3-}$ in neutral condition, 10 μL of $[^{64}Cu][Cu^{I}(BCS)_2]^{3-}$ (100 kBq, BCS concentration: 200 μM) was diluted with 90 μL of 100 mM phosphate buffer (pH 7.4). The stability of $[^{64}Cu][Cu^{I}(BCS)_2]^{3-}$ in human plasma was also evaluated as follows. To 85 μL of human plasma (male plasma, Sigma-Aldrich), 5 μL of 0.1 M $NaHCO_3$ was added to adjust the pH to 7.4. Then 10 μL of $[^{64}Cu][Cu^{I}(BCS)_2]^{3-}$ solution (100 kBq, BCS concentration 200 μM) was added. In addition, Ten microliter of $[^{64}Cu][Cu^{I}(BCS)_2]^{3-}$ solution (25 kBq, BCS concentration: 200 μM) was diluted with 90 μL of 100 mM phosphate buffer (pH 7.4) containing 20 μM of Fe^{3+}, 15 μM of Zn^{2+}, or 20 μM of Fe^{3+} and 15 μM of Zn^{2+}. The phosphate buffer containing Fe^{3+} or Zn^{2+} was adjusted by diluting iron (III) chloride (Sigma-Aldrich) or zinc (II) chloride with 100 mM phosphate buffer (pH 7.4). Each solution was incubated at 37°C for 30 min, and percentages of the intact complex were analyzed by RP-TLC (Table 1).

3 Results

3.1 Reactions of $[^{nat}Cu][Cu^{I}(BCA)_2]^{3-}$ and $[^{nat}Cu][Cu^{I}(BCS)_2]^{3-}$ with ROS

As shown in Figure 3, the generation of each ROS was separately validated by commercially available fluorescent reagents. Figure 4 summarizes the changes in the absorbance after the reaction of $[^{nat}Cu][Cu^{I}(BCA)_2]^{3-}$ and $[^{nat}Cu][Cu^{I}(BCS)_2]^{3-}$ with each ROS. After $[^{nat}Cu][Cu^{I}(BCA)_2]^{3-}$ was reacted with $^{\cdot}OH$, LOOH, $O_2^{\cdot-}$ and H_2O_2, the absorbance as percentage of control decreased to 53 ± 1%, 19 ±

316 1%, 77 ± 3%, and 76 ± 0%, respectively. After $[^{nat}Cu][Cu^{I}(BCS)_2]^{3-}$ was reacted with ·OH, LOOH,
317 $O_2^{\bullet-}$ and H_2O_2, the absorbance as percentage of control decreased to 29 ± 2%, 26 ± 5%, 87 ± 2% and
318 85 ± 3%, respectively. Only the value of $O_2^{\bullet-}$ was not significantly different from that of the control
319 group.

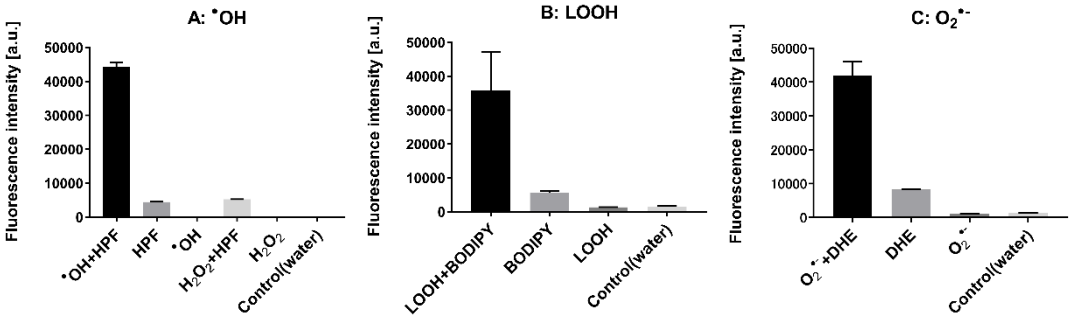

320

321 **Fig. 3**. The generation of each ROS was validated by commercially available fluorescence reagents.
322 Each bar represents mean ± SD (n = 3).
323

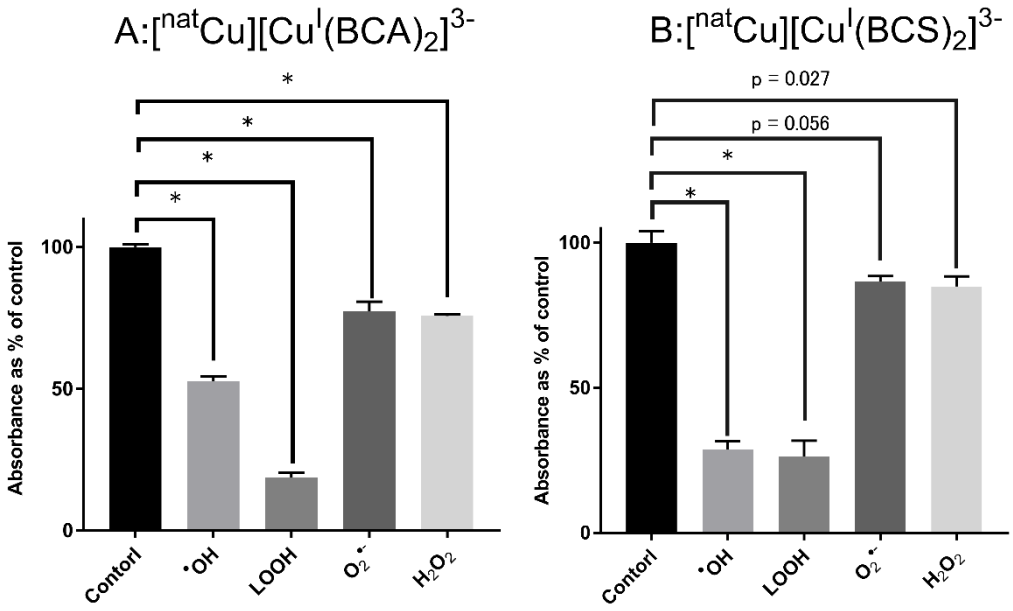

324

325 **Fig. 4**. The reactivities of (A) $[^{nat}Cu][Cu^{I}(BCA)_2]^{3-}$ and (B) $[^{nat}Cu][Cu^{I}(BCS)_2]^{3-}$ with four different
326 kinds of ROS. Each bar represents mean ± SD (n = 3). The statistical analyses were performed using
327 one way ANOVA followed by Dunnet's multiple comparison test. Asterisk indicates $p < 0.001$.
328

329 ### 3.2 Synthesis of $[^{64}Cu][Cu^{I}(BCA)_2]^{3-}$ and $[^{64}Cu][Cu^{I}(BCS)_2]^{3-}$

330 Figure 5 shows RP-TLC images of $[^{64/nat}Cu][Cu^{I}(BCA)_2]^{3-}$ and $[^{64/nat}Cu][Cu^{I}(BCS)_2]^{3-}$ after the
331 synthesis. Fluorescence spots were visualized by excitation with 365 nm UV. The Rf values of major

radioactive spots were identical to those of corresponding non-radioactive copper complexes. Moreover, ^{64}Cu-labeled complexes showed the same retention times in the HPLC analyses as their non-radioactive copper complexes (Figures S5 and S8). These results indicate that $[^{64}Cu][Cu^{I}(BCA)_2]^{3-}$ and $[^{64}Cu][Cu^{I}(BCS)_2]^{3-}$ were successfully synthesized. The radiochemical yields of $[^{64}Cu][Cu^{I}(BCA)_2]^{3-}$ and $[^{64}Cu][Cu^{I}(BCS)_2]^{3-}$ determined by the TLC analyses were 44 ± 3% and 86 ± 1%, respectively (n = 3). The radiochemical yield of $[^{64}Cu][Cu^{II}(DOTA)]^{2-}$ was 96 ± 1% (n = 3).

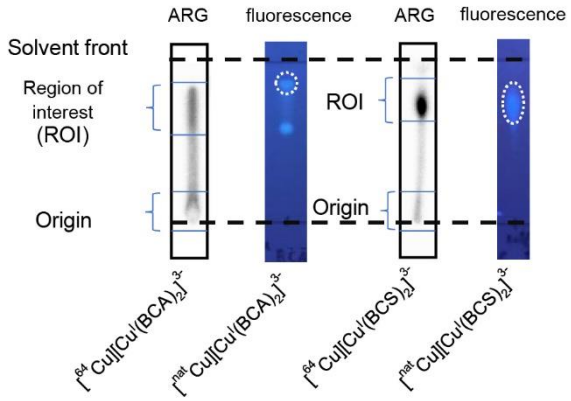

Fig. 5. Representative TLC analyses of $[^{64}Cu][Cu^{I}(BCA)_2]^{3-}$, $[^{nat}Cu][Cu^{I}(BCA)_2]^{3-}$, $[^{64}Cu][Cu^{I}(BCS)_2]^{3-}$, and $[^{nat}Cu][Cu^{I}(BCS)_2]^{3-}$. The spots of copper-64 complexes were visualized by ARG, and those of natural copper complexes were visualized by fluorescence signal (excitation wavelength was 365 nm).

3.3 Dilution stability of $[^{64}Cu][Cu^{I}(BCA)_2]^{3-}$ and $[^{64}Cu][Cu^{I}(BCS)_2]^{3-}$

Figure 6 shows the percentages of the intact $[^{64}Cu][Cu^{I}(BCA)_2]^{3-}$ and $[^{64}Cu][Cu^{I}(BCS)_2]^{3-}$ after dilution with acetate buffer. The percentages of the intact complexes decreased upon dilution, and radioactivity at the origin increased. After 100-hold dilution, the percentage of intact $[^{64}Cu][Cu^{I}(BCA)_2]^{3-}$ and $[^{64}Cu][Cu^{I}(BCS)_2]^{3-}$ decreased to 2 ± 3% and 53 ± 3%, respectively. In contrast, the percentage of intact $[^{64}Cu][Cu^{II}(DOTA)]^{2-}$ did not change even after 100-fold dilution (99.3 ± 0.2%).

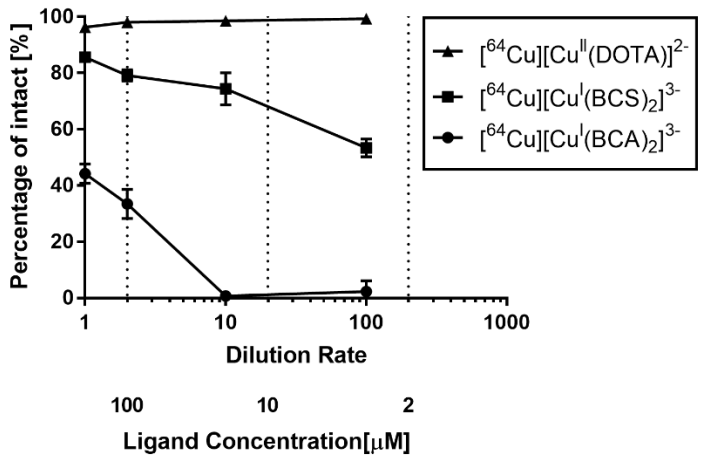

Fig. 6. The stability of $[^{64}Cu][Cu^{I}(BCA)_2]^{3-}$, $[^{64}Cu][Cu^{I}(BCS)_2]^{3-}$, and $[^{64}Cu][Cu^{II}(DOTA)]^{2-}$ against dilution. Each bar represents mean ± SD (n = 3).

3.4 Reaction of $[^{64}Cu][Cu^{I}(BCS)_2]^{3-}$ with ROS

Figures 7A and 7B show TLC images and percentages of radioactivity at the origin (% origin) after the reaction of $[^{64}Cu][Cu^{I}(BCS)_2]^{3-}$ with four different ROS and enzymes alone. After the reaction with ·OH, LOOH, $O_2^{\cdot-}$ and H_2O_2, 67 ± 2%, 44 ± 13%, 22 ± 3%, and 4 ± 1% of the radioactivity was observed at the origin, respectively. The % origin after the reaction with ·OH and LOOH were significantly different from the control group. On the other hand, the % origin after the reaction with $O_2^{\cdot-}$ and H_2O_2 were not significantly different between the control group. When $[^{64}Cu][Cu^{I}(BCS)_2]^{3-}$ was diluted 10 fold (control), 11 ± 3 % of the radioactivity was observed at the origin. The % origin did not change after incubation with peroxidase or lipoxygenase.

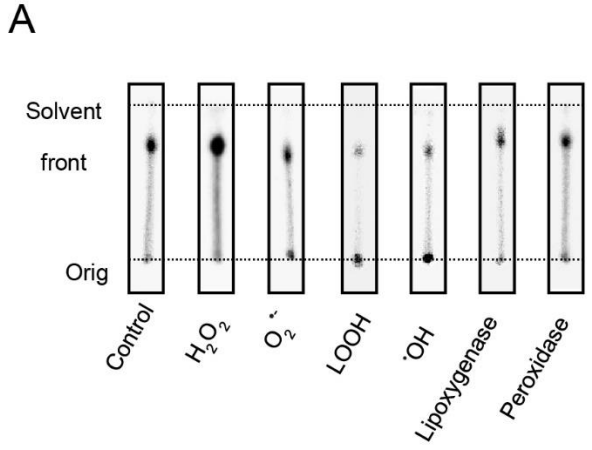

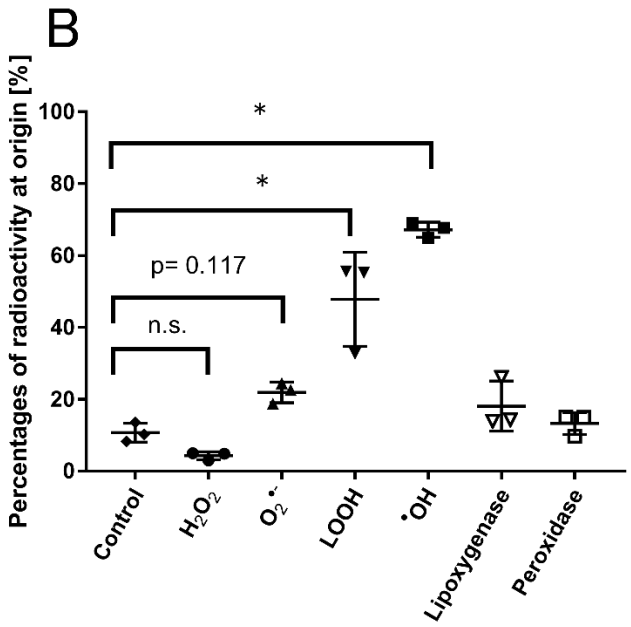

Fig. 7. The reactivity of $[^{64}Cu][Cu^{I}(BCS)_2]^{3-}$ with each ROS. (A) Representative TLC analyses after the incubation of $[^{64}Cu][Cu^{I}(BCS)_2]^{3-}$ with each ROS. (B) The percentages of radioactivity at origin (% origin) determined by the TLC analyses. Each bar represents mean ± SD (n = 3). The statistical analyses were performed using one way ANOVA followed by Dunnet's multiple comparison test. n.s. indicates not significant, and asterisk indicates $p < 0.0001$.

3.5 Cellular uptake of $[^{64}Cu][Cu^{I}(BCS)_2]^{3-}$

Figure 8A shows fluorescence images of HT-1080 cells stained with BODIPY C11 581/591 and its oxidized form, Ox-BODIPY C11, after IKE alone or IKE + Fer-1 treatment. In the IKE-treated group, the fluorescence signal of BODIPY C11 decreased and that of Ox-BODIPY C11 increased compared to the control group, demonstrating the formation of lipid peroxides by the IKE treatment. On the other hand, the fluorescence signal of Ox-BODIPY C11 was reduced by the co-incubation with Fer-1. Figure 8B shows the results of cellular uptake of $[^{64}Cu][Cu^{I}(BCS)_2]^{3-}$ to HT-1080 cells in three different conditions. The uptake of $[^{64}Cu][Cu^{I}(BCS)_2]^{3-}$ significantly increased by approximately 30% in the IKE-treated group (54 ± 2 %Dose/mg protein) compared to the control group (42 ± 2 %Dose/mg protein). In addition, the increased uptake was reduced by the treatment with Fer-1 (47 ± 5 %Dose/mg protein), a similar tendency observed in the fluorescence observation.

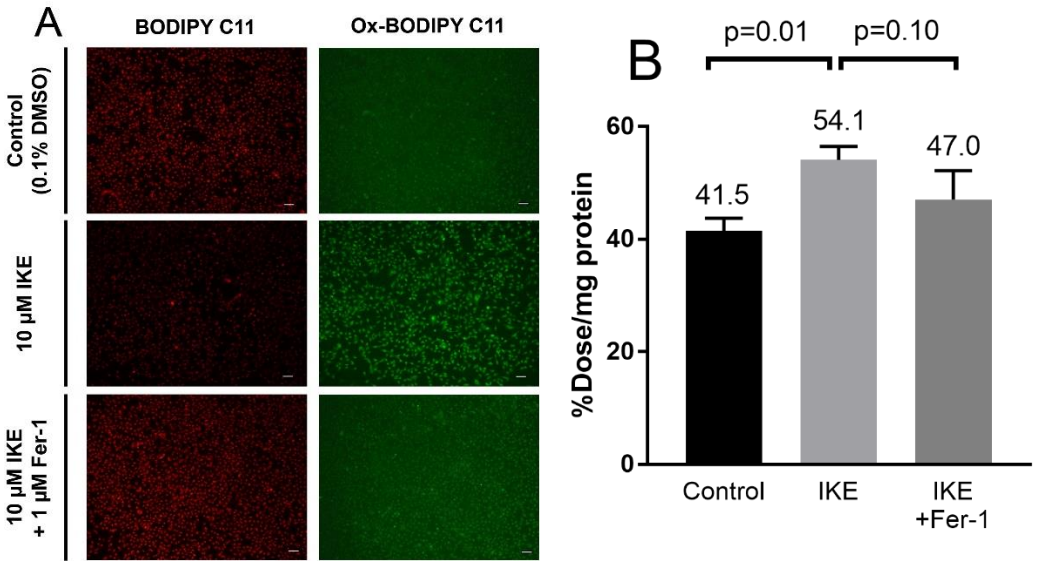

Fig. 8. (A) Representative fluorescence microscopy images of HT-1080 cells stained with BODIPY C11 (Left) and Ox-BODIPY C11 (Right). In the control group (top), IKE group (middle), and IKE + Fer-1 group (bottom), the cells were incubated with 0.1% DMSO, 10 μM IKE, 10 μM IKE + 1 μM Fer-1, respectively. Scale bar = 100 μm. (B) Cellular uptake of $[^{64}Cu][Cu^{I}(BCS)_2]^{3-}$ in the control, IKE, and IKE + Fer-1 group after 30 min incubation at 37°C. Each bar represents mean ± SD (n = 3). Statistical analysis was performed using one way ANOVA followed by Dunnet's multiple comparison test.

3.6 Stability of $[^{64}Cu][Cu^{I}(BCS)_2]^{3-}$ in neutral solution and human plasma

The intact ratios after incubation of $[^{64}Cu][Cu^{I}(BCS)_2]^{3-}$ in the neutral buffer and human plasma were 78 ± 2% (n = 3) and 9 ± 5% (n = 3), respectively. After incubation in human plasma, 88 ± 2% of radioactivity was detected at the origin (n = 3). The intact ratios after incubation of $[^{64}Cu][Cu^{I}(BCS)_2]^{3-}$ in 0.1 M phosphate buffer (pH 7.4) containing Fe^{3+}, Zn^{2+}, and both were 69 ± 2% (n = 3), 71 ± 1% (n = 3) and 73 ± 2 % (n = 3), respectively. Representative TLC images are shown in Figure 9.

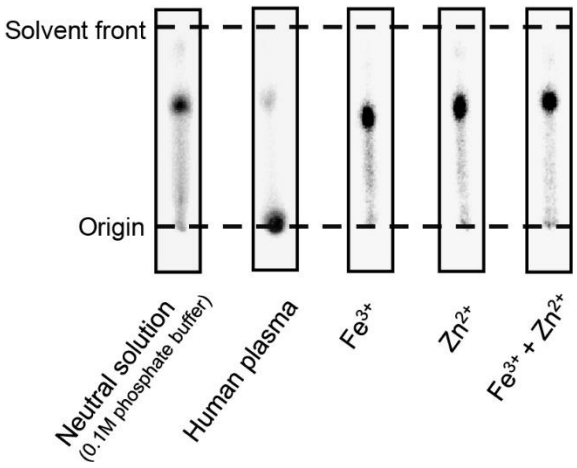

Fig. 9. Representative TLC analyses after the incubation of $[^{64}Cu][Cu^{I}(BCS)_2]^{3-}$ in 0.1 M phosphate buffer (pH 7.4), human plasma, and 0.1 M phosphate buffer (pH 7.4) containing Fe^{3+}, Zn^{2+}, or both. The final concentrations of Fe^{3+} and Zn^{2+} were 18 μM and 13.5 μM. respectively.

4 Discussion

In this study, we conducted several experiments to prove our hypothesis that PET imaging of ROS would be possible by using chelators that form a stable complex with Cu^{I} but not with Cu^{II}, based on metabolic trapping. As model chelators of such a property, we selected BCA and BCS, whose stability constant with Cu^{I} and Cu^{II} has been previously determined (Table 3). These two chelators form very stable complexes with Cu^{I} but not with Cu^{II}, and their copper (I) complexes are routinely used for protein quantification assay [24].

At first, we synthesized $[^{nat}Cu][Cu^{I}(BCA)_2]^{3-}$ and $[^{nat}Cu][Cu^{I}(BCS)_2]^{3-}$ and evaluated their reactivity with four different kinds of ROS (·OH, LOOH, $O_2^{\cdot-}$, and H_2O_2). We selected these ROS because they are relevant to different diseases and have different redox potentials (Table 4). Specifically, ·OH and LOOH are involved in ferroptosis, an iron-dependent cell death [25]. $O_2^{\cdot-}$ and H_2O_2 are involved in cancer [26] and mitochondrial dysfunction diseases [27]. We set the final concentration of ROS, which is defined by the concentration of substrate, to be 1 mM following a literature [17]. Since $[^{nat}Cu][Cu^{I}(BCA)_2]^{3-}$ and $[^{nat}Cu][Cu^{I}(BCS)_2]^{3-}$ have a characteristic absorption peak at 562 and 492 nm, respectively [22], [23], percent of the intact complexes was evaluated by measuring the changes in their absorption values. As expected, both $[^{nat}Cu][Cu^{I}(BCA)_2]^{3-}$ and $[^{nat}Cu][Cu^{I}(BCS)_2]^{3-}$ substantially decomposed by ·OH and LOOH, while $O_2^{\cdot-}$ and H_2O_2 reduced the intact ratio only slightly (Figure 4). This result is consistent with the redox potential of each ROS (Table 4).

We next synthesized $[^{64}Cu][Cu^{I}(BCA)_2]^{3-}$ and $[^{64}Cu][Cu^{I}(BCS)_2]^{3-}$ starting from $[^{64}Cu]Cu^{2+}$. Because $[^{64}Cu]Cu$ is obtained as a chemical form of $CuCl_2$, an appropriate reducing agent is needed to reduce Cu^{2+} to Cu^{+}. In this study, we used ascorbic acid as a reducing agent [28]. As shown in Figure 5, $[^{64}Cu][Cu^{I}(BCS)_2]^{3-}$ was obtained with a much higher radiochemical yield than $[^{64}Cu][Cu^{I}(BCA)_2]^{3-}$.

Furthermore, the radioactive spot of $[^{64}Cu][Cu^{I}(BCA)_2]^{3-}$ on the TLC (Figure 5) was somewhat indistinctive, suggesting that $[^{64}Cu][Cu^{I}(BCA)_2]^{3-}$ had partially decomposed during the development on TLC. This apparently lower stability of $[^{64}Cu][Cu^{I}(BCA)_2]^{3-}$ could be attributed to the lower stability constant of the copper (I) complex with BCA (Table 3). We also evaluated the stability of $[^{64}Cu][Cu^{I}(BCA)_2]^{3-}$ and $[^{64}Cu][Cu^{I}(BCS)_2]^{3-}$ against dilution by acetate buffer (Figure 6) and found a similar result that $[^{64}Cu][Cu^{I}(BCA)_2]^{3-}$ was much less stable than $[^{64}Cu][Cu^{I}(BCS)_2]^{3-}$. This inferior stability of $[^{64}Cu][Cu^{I}(BCA)_2]^{3-}$ against dilution could also be attributed to its lower stability constant (Table 2). In addition, because $[^{64}Cu][Cu^{I}(BCA)_2]^{3-}$ is a tetrahedral complex, and acetate ion are known to coordinate to Cu^{+} [29], an associative pathway might be responsible for the decomposition upon dilution. In contrast, $[^{64}Cu][Cu^{II}(DOTA)]^{2-}$, which is an octahedral copper (II) complex [30] with a stability constant of 22.3, showed excellent stability against dilution (Figure 6), suggesting that coordination number and geometry have a significant impact on kinetic inertness of copper complexes.

Table 3 Stability Constants for $[Cu^{I}(BCA)_2]^{3-}$, $[Cu^{I}(BCS)_2]^{3-}$ and $[Cu^{II}(DOTA)]^{2-}$.

Ligand	Stability constant: $[Cu^{I}(L)_2]^{+}$	Stability constant: $[Cu^{II}(L)_2]^{2+}$	References
BCA	17.2	8.2	[31]
BCS	20.81	12.42	[23]
DOTA	-	22.3	[32]

Because $[^{64}Cu][Cu^{I}(BCS)_2]^{3-}$ exhibited higher radiochemical yield and superior stability against dilution, we evaluated the reactivity of $[^{64}Cu][Cu^{I}(BCS)_2]^{3-}$ with ·OH, LOOH, $O_2^{\cdot-}$, and H_2O_2. As $[^{64}Cu]Cu^{2+}$ was detected at the origin of TLC, the % origin can be considered as a ratio of released $[^{64}Cu]Cu^{2+}$ from $[^{64}Cu][Cu^{I}(BCS)_2]^{3-}$ upon oxidation. As shown in Figure 7, the % origin increased when $[^{64}Cu][Cu^{I}(BCS)_2]^{3-}$ was reacted with ·OH and LOOH, while the reaction with $O_2^{\cdot-}$ and H_2O_2 did not significantly increase its value. Again, this trend is consistent with the redox potential of each ROS (Table4). In addition, because the % origin did not change when $[^{64}Cu][Cu^{I}(BCS)_2]^{3-}$ was reacted with enzymes alone (peroxidase without H_2O_2, lipoxygenase without linoleic acid), the increase in the % origin can be attributed to the release of $[^{64}Cu]Cu^{2+}$ but not to the formation of ^{64}Cu-enzyme complexes. These results suggest that $[^{64}Cu][Cu^{I}(BCS)_2]^{3-}$ may be used for detecting high-redox-potential ROS such as ·OH and LOOH.

Table 4 Redox potentials of ROS and complexes used in this study.

ROS/complex	Redox potential [V/NHE]	Reference
$^{\bullet}OH + H^{+}/H_2O$ ($1e^{-}$)	2.3	[33]
$LOOH + H^{+}/LO^{\bullet}+H_2O$ ($1e^{-}$)	1.9	[34]

$LOOH+2H^+/LOH+H_2O$ ($2e^-$)	1.7	[34]
$LOO^\bullet+H^+/LOOH$ ($1e^-$)	0.77-1.44	[35]
$O_2^{\bullet-}/H_2O_2$ ($1e^-$)	0.9	[33]
$[Cu^{II}(BCS)_2]^{2-}/[Cu^{I}(BCS)_2]^{3-}$ ($1e^-$)	0.66	[31]
$[Cu^{II}(BCA)_2]^{2-}/[Cu^{I}(BCA)_2]^{3-}$ ($1e^-$)	0.65	[31]
H_2O_2/H_2O+OH^- ($1e^-$)	0.38	[36]

458 $1e^-$: one electron oxidation, $2e^-$: two electron oxidation, $LO^\bullet$: lipid hydroxyl radical, $LOO^\bullet$: lipid
459 peroxyl radical, LOH: lipid hydroxy, LOOH: lipid peroxide. LOOH is made from lipid peroxyl radical
460 [37].
461
462 The experimental condition of the above experiment is very simple: $[^{64}Cu][Cu^{I}(BCS)_2]^{3-}$ is mixed
463 with each ROS and the amount of $[^{64}Cu]Cu^{2+}$ released from $[^{64}Cu][Cu^{I}(BCS)_2]^{3-}$ is evaluated. However,
464 actual cellular processes involving the production of ROS are much more complicated. Especially, it
465 is highly important to consider the influence of re-reduction of the oxidized complex by the
466 surrounding reductase enzymes and antioxidants [38]. Therefore, cell-based experiments are
467 indispensable to evaluate the efficacy of imaging agents that rely on metabolic trapping. We thereby
468 evaluated the uptake of $[^{64}Cu][Cu^{I}(BCS)_2]^{3-}$ to cancer cells that were treated with IKE, a ferroptosis
469 inducer [39]. The HT-1080 cell line, known to be susceptible to ferroptosis, was used in this
470 experiment [25], and Fer-1 was employed as a ferroptosis inhibitor [40]. At first, we confirmed the
471 formation of LOOH, a hallmark of ferroptosis, using a commercially available fluorescent probe
472 BODIPY C11. As shown in Figure 8A, IKE treatment led to the formation of LOOH, and its formation
473 was suppressed by the co-treatment with Fer-1 to the level of the control group. This result indicates
474 that IKE-treated HT-1080 cells can be a good model to evaluate the ROS-specific cellular uptake of
475 novel imaging agents. Hence, we evaluated the uptake of $[^{64}Cu][Cu^{I}(BCS)_2]^{3-}$ to HT-1080 cells under
476 the same conditions as the fluorescent experiment. As shown in Figure 8B, the uptake of
477 $[^{64}Cu][Cu^{I}(BCS)_2]^{3-}$ in the IKE-treated group was significantly higher than the control group.
478 Furthermore, this increased uptake of $[^{64}Cu][Cu^{I}(BCS)_2]^{3-}$ was reduced by the co-treatment with Fer-
479 1, suggesting that the uptake of $[^{64}Cu][Cu^{I}(BCS)_2]^{3-}$ to IKE-treated cells was LOOH specific.
480 It is important to note that $[Cu^{I}(BCS)_2]^{3-}$ is considered not to cross the cell membrane due to its
481 negative charge in neutral environment. On the other hand, it was reported that lipid peroxidation
482 enhanced cell membrane permeability due to the loss of membrane integrity [41], [42]. Therefore, it
483 is quite possible that $[^{64}Cu][Cu^{I}(BCS)_2]^{3-}$ was taken up into the cell through the impaired membrane,
484 followed by oxidation by ROS and trapped inside or in the membrane of the cell. At the same time,
485 however, it is also possible that $[^{64}Cu][Cu^{I}(BCS)_2]^{3-}$ was merely taken up into the cell and trapped
486 there without oxidation. Thus, it is not easy to interpret whether the enhanced cellular uptake was
487 caused by the production of ROS, enhanced membrane permeability, or both, which is a major

shortcoming of $[^{64}Cu][Cu^{I}(BCS)_2]^{3-}$ as a ROS imaging agent. To address this issue, the development of novel ^{64}Cu-labeled complexes that can freely cross the intact cell membrane, like $[^{64}Cu]$Cu-ATSM, would be essential.

We lastly evaluated the stability of $[^{64}Cu][Cu^{I}(BCS)_2]^{3-}$ in a neutral condition and biological condition. As shown in Figure 9, $[^{64}Cu][Cu^{I}(BCS)_2]^{3-}$ was stable in a neutral buffer, but decomposed almost completely after incubated with human plasma for 30 min. This low stability could be attributed to the substitution of BCS in $[^{64}Cu][Cu^{I}(BCS)_2]^{3-}$ with proteins in human plasma. Indeed, human plasma is rich in proteins that have a very high affinity to copper [43]. On the other hand, Fe^{3+} and Zn^{2+}, both present in plasma, can also form stable complexes with phenanthroline [44], [45], a coordinating moiety to Cu (I) in BCS. Hence, to clarify whether these metal ions also contributed to the instability of $[^{64}Cu][Cu^{I}(BCS)_2]^{3-}$, we evaluated the stability of the copper complex in a neutral buffer containing plasma-equivalent concentrations of Fe^{3+} or Zn^{2+} [46], [47]. As shown in Figure 9, $[^{64}Cu][Cu^{I}(BCS)_2]^{3-}$ was stable under these conditions, indicating that Fe^{3+} or Zn^{2+} was not responsible for the instability of $[^{64}Cu][Cu^{I}(BCS)_2]^{3-}$ in human plasma.

Over the last several decade, intensive efforts have been made to develop chelators that form stable complexes with both Cu (II) and Cu (I) [48], [49]. On the other hand, much less attention has been paid to chelators that have selective affinity to Cu (I) [50]. Thus, there should still be sufficient scope to develop novel copper (I) selective ligands for PET imaging of ROS. The present results suggest that associative pathway may be responsible for the decomposition of $[^{64}Cu][Cu^{I}(BCS)_2]^{3-}$ in human plasma. Therefore, employing bulky ligands might be effective to prevent the decomposition via associative pathway and provide copper (I) complexes with improved stability in biological condition [51].

5 Conclusion

In this study, we demonstrated that PET imaging of ROS would be possible by using a chelator that forms a stable complex with Cu (I) but not with Cu (II), based on metabolic trapping. In a proof-of-concept experiment, $[^{64}Cu][Cu^{I}(BCS)_2]^{3-}$ showed enhanced uptake to cancer cells with elevated ROS levels. Although improvements of the membrane permeability and stability of copper (I) complexes in biological conditions are necessary for successful in vivo application, the present results pave the way for the development of novel ^{64}Cu-labeled complexes for PET imaging of ROS. Taken together, the present study warrants further investigation on the application of copper (I) selective ligands for non-invasive PET imaging of ROS through metabolic trapping.

Conflict of Interest Statement

The authors declare that they have no conflict of interest.

Acknowledgement

This work was supported in part by JSPS KAKENHI grant number 21K19433.

Supplementary data

ESI-MS of $[^{nat}Cu][Cu^{I}(BCA)_2]^{3-}$ and $[^{nat}Cu][Cu^{I}(BCS)_2]^{3-}$

HPLC chromatograms of BCA, BCS, $[^{nat/64}Cu][Cu^{I}(BCA)_2]^{3-}$, and $[^{nat/64}Cu][Cu^{I}(BCS)_2]^{3-}$

Abbreviations (a to z)

ARG, autoradiography; BCA, bicinchoninic acid disodium salt; BCS, disodium bathocuproine disulfonate acid disodium salt; DMSO, dimethyl sulfoxide; DOTA, 1,4,7,10-tetraazacyclododecane-1,4,7,10-tetraacetic acid; Fer-1, ferrostatin-1; HBSS, Hank's balanced salt solution; HPLC, High Performance Liquid Chromatography; HRP, horseradish peroxidase; ICP, inductively coupled plasma; IKE, imidazole ketone erastin; $LO^{\bullet}$, lipid hydroxyl radical; LOH, lipid hydroxy; $LOO^{\bullet}$: lipid peroxyl radical; LOOH, lipid peroxide; NHE, normal hydrogen electrode; $O_2^{\bullet-}$, superoxide; $^{\bullet}OH$, hydroxyl radical; PET, positron emissions tomography; RP-TLC, reverse phase thin-layer chromatography; ROS, reactive oxygen species; SD, standard deviation; SDS, sodium dodecyl sulfate; TLC, thin-layer chromatography

References

[1] Sies H and Jones DP. Reactive oxygen species (ROS) as pleiotropic physiological signalling agents. Nature Reviews Molecular Cell Biology 2020;21:363-83.

[2] Liou GY and Storz P. Reactive oxygen species in cancer. Free Radic Res 2010;44:479-96.

[3] Sahoo BM, Banik BK, Borah P, and Jain A. Reactive Oxygen Species (ROS): Key Components in Cancer Therapies. Anticancer Agents Med Chem 2022;22:215-22.

[4] Yang H, Villani RM, Wang H, Simpson MJ, Roberts MS, Tang M, et al. The role of cellular reactive oxygen species in cancer chemotherapy. J Exp Clin Cancer Res 2018;37:266.

[5] Chen HHW and Kuo MT. Improving radiotherapy in cancer treatment: Promises and challenges. Oncotarget 2017;8:62742-58.

[6] Hou C, Hsieh C-J, Li S, Lee H, Graham TJ, Xu K, et al. Development of a Positron Emission Tomography Radiotracer for Imaging Elevated Levels of Superoxide in Neuroinflammation. ACS Chem. Neurosci. 2018;9:578-86.

[7] Al-Karmi S, Albu SA, Vito A, Janzen N, Czorny S, Banevicius L, et al. Preparation of an 18F-Labeled

Hydrocyanine Dye as a Multimodal Probe for Reactive Oxygen Species. Chemistry – A European Journal 2017;23:254-8.

[8] Damuka N, Bashetti N, Mintz A, Bansode AH, Miller M, Krizan I, et al. [18F]KS1, a novel ascorbate-based ligand images ROS in tumor models of rodents and nonhuman primates. Biomedicine & Pharmacotherapy 2022;156:113937.

[9] Pisaneschi F, Gammon ST, Paolillo V, Qureshy SA, and Piwnica-Worms D. Imaging of innate immunity activation in vivo with a redox-tuned PET reporter. Nature Biotechnology 2022;40:965-73.

[10] Egami H, Nakagawa S, Katsura Y, Kanazawa M, Nishiyama S, Sakai T, et al. 18F-Labeled dihydromethidine: positron emission tomography radiotracer for imaging of reactive oxygen species in intact brain. Org. Biomol. Chem. 2020;18:2387-91.

[11] Price EW and Orvig C. Matching chelators to radiometals for radiopharmaceuticals. Chem. Soc. Rev. 2014;43:260-90.

[12] Sun Y, Anderson CJ, Pajeau TS, Reichert DE, Hancock RD, Motekaitis RJ, et al. Indium(III) and Gallium(III) Complexes of Bis(aminoethanethiol) Ligands with Different Denticities: Stabilities, Molecular Modeling, and in Vivo Behavior. Journal of Medicinal Chemistry 1996;39:458-70.

[13] Bailey GA, Price EW, Zeglis BM, Ferreira CL, Boros E, Lacasse MJ, et al. H2azapa: a Versatile Acyclic Multifunctional Chelator for 67Ga, 64Cu, 111In, and 177Lu. Inorganic Chemistry 2012;51:12575-89.

[14] Sivapackiam J, Liao F, Zhou D, Shoghi KI, Gropler RJ, Gelman AE, et al. Galuminox: Preclinical validation of a novel PET tracer for non-invasive imaging of oxidative stress in vivo. Redox Biology 2020;37:101690.

[15] Ikawa M, Okazawa H, Nakamoto Y, and Yoneda M. PET Imaging for Oxidative Stress in Neurodegenerative Disorders Associated with Mitochondrial Dysfunction. Antioxidants; 2020.

[16] Saito Y, Nishikawa M, and Tsubomura T. Water-soluble copper(<scp>i</scp>) complexes bearing 2,2′-bicinchoninic acid dipotassium salt with red-light absorption and repeatable colour change upon freezing operation. New Journal of Chemistry 2019;43:277-83.

[17] Chu W, Chepetan A, Zhou D, Shoghi KI, Xu J, Dugan LL, et al. Development of a PET radiotracer for non-invasive imaging of the reactive oxygen species, superoxide, in vivo. Org. Biomol. Chem. 2014;12:4421-31.

[18] Azuma R, Yamasaki T, Sano K, Munekane M, Matsuoka Y, Yamada K-i, et al. A radioiodinated nitroxide probe with improved stability against bioreduction for in vivo detection of lipid radicals. Free Radical Biology and Medicine 2021;163:297-305.

[19] Fink B, Laude K, McCann L, Doughan A, Harrison DG, and Dikalov S. Detection of intracellular superoxide formation in endothelial cells and intact tissues using dihydroethidium and an HPLC-based assay. Am J Physiol Cell Physiol 2004;287:C895-902.

[20] Setsukinai K-i, Urano Y, Kakinuma K, Majima HJ, and Nagano T. Development of Novel Fluorescence Probes That Can Reliably Detect Reactive Oxygen Species and Distinguish Specific Species*210. Journal

of Biological Chemistry 2003;278:3170-5.
[21] Aldini G, Yeum K-J, Russell RM, and Krinsky NI. A method to measure the oxidizability of both the aqueous and lipid compartments of plasma. Free Radical Biology and Medicine 2001;31:1043-50.
[22] Walker JM. The bicinchoninic acid (BCA) assay for protein quantitation. The protein protocols handbook 2009:11-5.
[23] Bagchi P, Morgan MT, Bacsa J, and Fahrni CJ. Robust Affinity Standards for Cu(I) Biochemistry. Journal of the American Chemical Society 2013;135:18549-59.
[24] Wiechelman KJ, Braun RD, and Fitzpatrick JD. Investigation of the bicinchoninic acid protein assay: Identification of the groups responsible for color formation. Analytical Biochemistry 1988;175:231-7.
[25] Dixon SJ, Lemberg KM, Lamprecht MR, Skouta R, Zaitsev EM, Gleason CE, et al. Ferroptosis: an iron-dependent form of nonapoptotic cell death. Cell 2012;149:1060-72.
[26] Aykin-Burns N, Ahmad IM, Zhu Y, Oberley LW, and Spitz DR. Increased levels of superoxide and H2O2 mediate the differential susceptibility of cancer cells versus normal cells to glucose deprivation. Biochem J 2009;418:29-37.
[27] Brand MD. Mitochondrial generation of superoxide and hydrogen peroxide as the source of mitochondrial redox signaling. Free Radical Biology and Medicine 2016;100:14-31.
[28] Riedinger A, Avellini T, Curcio A, Asti M, Xie Y, Tu R, et al. Post-Synthesis Incorporation of 64Cu in CuS Nanocrystals to Radiolabel Photothermal Probes: A Feasible Approach for Clinics. Journal of the American Chemical Society 2015;137:15145-51.
[29] Mounts RD, Ogura T, and Fernando Q. Crystal structure of copper(I) acetate. Inorganic Chemistry 1974;13:802-5.
[30] Boswell CA, Sun X, Niu W, Weisman GR, Wong EH, Rheingold AL, et al. Comparative in Vivo Stability of Copper-64-Labeled Cross-Bridged and Conventional Tetraazamacrocyclic Complexes. J. Med. Chem. 2004;47:1465-74.
[31] Chen D, Wang X, He Y, Kai T, Li Z, Xiang J, et al. Studies of Electrode Reactions and Coordination Geometries of Cu(I) and Cu(II) Complexes with Bicinchoninic Acid. Electroanalysis 2018;30:479-85.
[32] Sun X, Wuest M, Kovacs Z, Sherry AD, Motekaitis R, Wang Z, et al. In vivo behavior of copper-64-labeled methanephosphonate tetraaza macrocyclic ligands. J Biol Inorg Chem 2003;8:217-25.
[33] Wood PM. The Potential Diagram for Oxygen at Ph-7. Biochem J 1988;253:287-9.
[34] Koppenol WH. Oxyradical reactions: from bond-dissociation energies to reduction potentials. FEBS Letters 1990;264:165-7.
[35] Halliwell B and Gutteridge JM. Free radicals in biology and medicine: Oxford university press, USA,2015.
[36] Arnhold J, Furtmüller PG, and Obinger C. Redox properties of myeloperoxidase. Redox Report 2003;8:179-86.
[37] Girotti AW. Mechanisms of lipid peroxidation. Journal of Free Radicals in Biology & Medicine

1985;1:87-95.
[38] Murphy MP, Bayir H, Belousov V, Chang CJ, Davies KJA, Davies MJ, et al. Guidelines for measuring reactive oxygen species and oxidative damage in cells and in vivo. Nature Metabolism 2022;4:651-62.
[39] Zhang Y, Tan H, Daniels JD, Zandkarimi F, Liu H, Brown LM, et al. Imidazole Ketone Erastin Induces Ferroptosis and Slows Tumor Growth in a Mouse Lymphoma Model. Cell Chem Biol 2019;26:623-33.e9.
[40] Miotto G, Rossetto M, Di Paolo ML, Orian L, Venerando R, Roveri A, et al. Insight into the mechanism of ferroptosis inhibition by ferrostatin-1. Redox Biol 2020;28:101328.
[41] Pedrera L, Espiritu RA, Ros U, Weber J, Schmitt A, Stroh J, et al. Ferroptotic pores induce Ca2+ fluxes and ESCRT-III activation to modulate cell death kinetics. Cell Death & Differentiation 2021;28:1644-57.
[42] Riegman M, Sagie L, Galed C, Levin T, Steinberg N, Dixon SJ, et al. Ferroptosis occurs through an osmotic mechanism and propagates independently of cell rupture. Nature Cell Biology 2020;22:1042-8.
[43] Linder MC. Ceruloplasmin and other copper binding components of blood plasma and their functions: an update. Metallomics 2016;8:887-905.
[44] Brandt WW, Dwyer FP, and Gyarfas ED. Chelate Complexes of 1,10-Phenanthroline and Related Compounds. Chemical Reviews 1954;54:959-1017.
[45] Cooper MS, Ma MT, Sunassee K, Shaw KP, Williams JD, Paul RL, et al. Comparison of 64Cu-Complexing Bifunctional Chelators for Radioimmunoconjugation: Labeling Efficiency, Specific Activity, and in Vitro/in Vivo Stability. Bioconjugate Chemistry 2012;23:1029-39.
[46] Bernadette P. Marriott DFB, Virginia A. Stalling, Allison A. Yates. Present Knowledge in Nutrition: Basic Nutrition and Metabolism. 11 ed.: Academic Press,2020.
[47] Bennett P and Williamson C. Basic Science in Obstetrics and Gynaecology: A Textbook for MRCOG Part I: Churchill Livingstone,2010.
[48] Le Fur M, Beyler M, Le Poul N, Lima LMP, Le Mest Y, Delgado R, et al. Improving the stability and inertness of Cu(ii) and Cu(i) complexes with methylthiazolyl ligands by tuning the macrocyclic structure. Dalton Transactions 2016;45:7406-20.
[49] Woodin KS, Heroux KJ, Boswell CA, Wong EH, Weisman GR, Niu W, et al. Kinetic Inertness and Electrochemical Behavior of Copper(II) Tetraazamacrocyclic Complexes: Possible Implications for in Vivo Stability. European Journal of Inorganic Chemistry 2005;2005:4829-33.
[50] Bodio E, Boujtita M, Julienne K, Le Saec P, Gouin SG, Hamon J, et al. Synthesis and Characterization of a Stable Copper(I) Complex for Radiopharmaceutical Applications. ChemPlusChem 2014;79:1284-93.
[51] Alidori S, Gioia Lobbia G, Papini G, Pellei M, Porchia M, Refosco F, et al. Synthesis, in vitro and in vivo characterization of 64Cu(I) complexes derived from hydrophilic tris(hydroxymethyl)phosphane and 1,3,5-triaza-7-phosphaadamantane ligands. JBIC Journal of Biological Inorganic Chemistry 2008;13:307-15.